FLOMEKO 2022

Numerical investigation of boundary layer effects within cylindrical critical flow Venturi nozzles

S. Weiss[1], B. Mickan[2], J. Polansky[3], K. Oberleithner[4], M. Bär[1], and S. Schmelter[1]

[1]Physikalisch-Technische Bundesanstalt (PTB), Abbestr. 2-12, 10587 Berlin, Germany
[2]Physikalisch-Technische Bundesanstalt (PTB), Bundesallee 100, 38116 Braunschweig, Germany
[3]MECAS ESI, part of ESI Group, Brojova 2113, 32600 Pilsen, Czech Republic
[4]Institute of Fluid Dynamics and Technical Acoustics, Technische Universität Berlin, Müller-Breslau-Str. 8, 10623 Berlin, Germany
E-mail (corresponding author): sebastian.weiss@ptb.de

Abstract

This numerical study investigates the flow through a cylindrically shaped critical flow Venturi nozzle regarding the transitional behavior of the boundary layer inside the nozzle throat region. For the flow simulations, two different turbulence modeling approaches were used, and the simulation results were validated by comparison with experimental data. Characteristic quantities for describing the boundary layer development, namely the displacement and momentum thickness, were analyzed within the cylindrical part of the nozzle and compared with theoretical predictions based on integral methods for solving the boundary layer equations. Typical laminar and turbulent boundary layer flows could be classified depending on the Reynolds number, where the boundary layer curves show a self-similarity when multiplied by $\sqrt{Re}$ and $Re^{0.139}$, respectively. The shape factor, defined as the ratio of displacement to momentum thickness, was identified to indicate the transitional region of the nozzle flow. Thus, this parameter can help improving transitional turbulence models based on experimental data.

1. Introduction

Critical flow Venturi nozzles (CFVNs) are a state-of-the-art secondary standard widely used for gas flow measurements. The mass flow rate through the nozzle, and thus the discharge coefficient C_D as described by the ratio of actual to ideal mass flow rate, highly correlate with the boundary layer thickness inside the nozzle throat. The higher the boundary layer thickness, the smaller becomes the effective area of the flow, which leads to a reduction of the mass flow rate. Furthermore, the C_D value depends on the predominant boundary layer type (laminar or turbulent). Thus, a detailed analysis of the boundary layer development and the prediction of the laminar-to-turbulent transition inside the nozzle throat are crucial for the characterization of the flow and, hence, for a reliable prediction of the mass flow rate of critical nozzles.

According to the ISO 9300 standard [1], two nozzle types can be differentiated, the toroidal and the cylindrical nozzle. The toroidal nozzle has its critical diameter in one location, whereas for the cylindrical type, the nozzle throat encompasses a defined axial length (typically of one throat diameter d). Recent numerical studies by Ünsal et al. [2] and Wang et al. [3] investigated the transitional effects of the boundary layer for toroidal-shaped critical nozzles regarding the nozzle diameter and the influence of wall roughness, respectively. Lambert et al. [4] computationally studied the flow through cylindrical critical nozzles in both laminar and turbulent regimes using a one-equation turbulence model. However, in terms of cylindrical CFVNs no numerical data was found regarding the transitional behavior of the boundary layer flow. Hence, this study provides deeper insight into this topic using two different turbulence modeling approaches.

The simulation results of the two turbulent models are compared with corresponding experimental data in terms of the discharge coefficient. In comparison with theoretical predictions, the displacement and momentum thickness in the nozzle are analyzed as characteristic quantities to distinguish between laminar and turbulent boundary layer flows. Furthermore, special attention is paid to the shape factor as a potential indicator for the transitional region of the nozzle flow.

2. Methods

The computational domain of the cylindrical nozzle studied in this work is depicted in Figure 1. It consists of a 5° wedge sector of the nozzle to represent a two-dimensional axisymmetric flow. The inlet region encompasses a quarter circle with a radius of $2d$, where the throat diameter d is 1 mm. The outlet region has an extension of $8d$ in the axial (z) and radial (y) direction. The geometry of the nozzle is according to the ISO 9300 standard [1] and can be divided into a convergent, cylindrical, and divergent part.

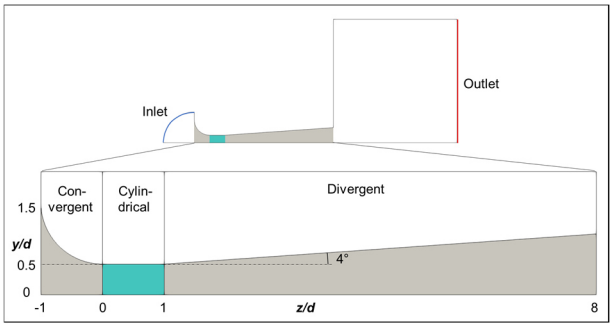

Figure 1: Computational domain of the cylindrical nozzle.

The numerical simulation has been conducted in OpenFOAM v2012 using the transient, compressible solver sonicFoam. Two different RANS turbulence models were used, namely the k-ω SST turbulence model [3] and the γ-Re_θ transitional model [6]. The second model extends the classical SST model by solving two additional transport equations for the intermittency γ and the momentum thickness Reynolds number Re_θ. The intermittency acts as a trigger at which turbulence production is activated, and the momentum thickness Reynolds number is based on experimental correlations regarding transition onset mainly in the field of aeronautics [6]. In this work, the default settings and correlations of the γ - Re_θ transitional model were used. For both models, the wall function nutkWallFunction of OpenFOAM was employed that applies a turbulence viscosity wall condition based on the local y^+ value. In the following, the two specific turbulence models will be referred to as "standard" and "transitional model", respectively.

For both models (standard and transitional), a set of ten different throat Reynolds numbers has been investigated, ranging from $2.6 \cdot 10^4$ to $1.3 \cdot 10^7$. The variation of the throat Reynolds number was realized by varying the total inlet pressure, according to the ISO 9300 [1]. The ratio of static outlet to total inlet pressure, also referred to as the back pressure ratio (BPR), was fixed to a value of 0.5 to allow for a critical flow through the nozzle. The total inlet temperature was kept constant at 300 K and the inlet turbulence intensity was set to 2%. For all calculations, the flowing fluid is air considered as a perfect gas. At the walls, no-slip boundary conditions were implemented.

For the k-ω SST model, a grid independence study was performed comparing three different refinement levels regarding the prediction of the discharge coefficient for different Reynolds numbers. Based on this study, a mesh with approximately 350,000 hexahedral cells was selected for all further flow simulations as the best compromise between accuracy and computational runtime. The mesh considers appropriate cell refinement towards the walls and flow regions where high gradients are expected, as in shock fronts. In addition, a y^+ value of 1 or below was used at the walls in the cylindrical part of the nozzle, as recommended in [6].

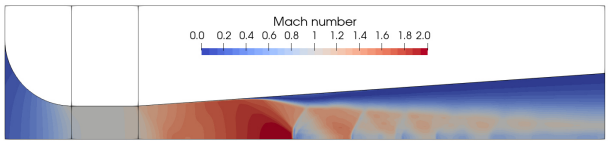

Figure 2: Mach number plot (transitional model at a throat Reynolds number of $2.6 \cdot 10^5$).

Figure 2 illustrates a typical Mach number distribution in the cylindrical nozzle as simulated with the transitional model at a Reynolds number of $2.6 \cdot 10^5$. The shock structures are located inside of the divergent part of the nozzle, which holds true for all regarded flow cases since the constant BPR of 0.5 is mainly responsible for the position of the shock structures. A Mach number of 1 (critical condition) is already reached in the cylindrical part. Hence, the flow phenomena occurring in the divergent part have negligible influence on the upstream flow behavior.

3. Results

In Figure 3 the discharge coefficients of the standard and transitional model for different Reynolds numbers are compared with experimental data from primary standard flow measurements of a smooth and a rough cylindrical nozzle according to the ISO 9300 [1]. The smooth nozzle is referenced as TF65 in [7] and was used at the National Metrology Institutes Physikalisch-Technische Bundesanstalt (PTB) and Laboratoire National de Métrologie et d'Essais (LNE). The rough nozzle was tested at PTB with a machined roughness Ra of 0.7 µm. Although the numerical models do not consider rough walls, a comparison with the tested nozzle is useful as the surface roughness has a negligible influence on the discharge coefficient in the laminar region (cf. [3]) at which the rough nozzle was measured.

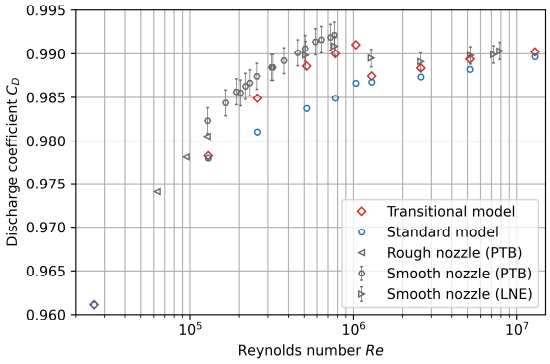

Figure 3: Discharge coefficients of the numerical simulation for different Reynolds numbers, compared with experimental data.

The experimental data indicates three distinguishable regimes of the nozzle flow. In the laminar range ($Re < 8 \cdot 10^5$), there is a steep increase in discharge coefficient with higher Reynolds numbers. In the

transitional region, $8 \cdot 10^5 < Re < 2 \cdot 10^6$, the C_D values slightly decrease until the discharge coefficients again increase in the turbulent range ($Re > 2 \cdot 10^6$), but with a smaller slope compared to the laminar part.

The standard model is able to predict the experimental data for higher Reynolds numbers above $2 \cdot 10^6$ and smaller Reynolds numbers below $2 \cdot 10^5$. However, it fails in the intermediate range.
The results of the transitional model, on the other hand, are in good agreement with the experiments throughout the entire Reynolds number range depicted. Especially in the intermediate range ($2 \cdot 10^5 < Re < 2 \cdot 10^6$), the improvements of the transitional model towards the standard model become notable. The immediate decrease in discharge coefficient at around $Re = 10^6$, as predicted by the transitional model, is a clear indication for the inherent change from laminar to turbulent behavior of the flow and is an estimate for the position of the transitional region. This correlates well with the experimental data, where the decrease of the C_D value is not as steep as in the simulation, but it is also located in the same Reynolds number range.

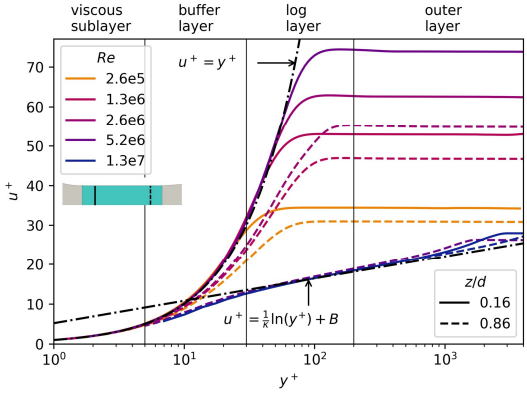

Figure 4: Dimensionless velocity profiles at two locations in the cylindrical part of the nozzle (transitional model).

Figure 4 depicts the dimensionless velocity profiles of the transitional model at two locations inside the cylindrical part of the nozzle. The two locations at a position of $z/d = 0.16$ and 0.86 are referred to by solid and dashed lines, respectively. Within the viscous sublayer ($y^+ < 5$), all curves coincide with $u^+ = y^+$. Outside of the viscous sublayer, two distinct curve characteristics can be distinguished corresponding to either a laminar or a turbulent boundary layer.

The laminar curves continue to follow the viscous sublayer line until they diverge from it and stagnate at a constant value of u^+. The higher the Reynolds number, the later the curves begin to diverge, thus reaching higher dimensionless velocities. The turbulent curves fall onto a second characteristic line, as described by the logarithmic law of the wall $u^+ = \kappa^{-1} \ln y^+ + B$ (for smooth walls, κ and B are 0.41 and 5.2, respectively). This line is a self-similar solution for turbulent velocity profiles in the log layer region ($30 < y^+ < 200$).

The trendline of the velocity profile at a Reynolds number of $5.2 \cdot 10^6$ can be categorized as laminar at z/d = 0.16 and as turbulent at z/d = 0.86, indicating a boundary layer transition inside the cylindrical part of the nozzle for this specific flow scenario. For lower Reynolds numbers, the boundary layer is laminar in the entire cylindrical part of the nozzle. For higher Reynolds numbers, the transitional model predicts a fully turbulent behavior in the nozzle throat.

For the standard turbulence model, all curves follow the turbulent trend (not shown in Figure 4 for reasons of clarity), indicating a turbulent boundary layer independent of the Reynolds number.

Two typical parameters to quantitatively describe the boundary layer are the displacement thickness δ_1 and the momentum thickness δ_2, which can be calculated as follows for a specific streamwise position at the wall

$$\delta_1 = \int_0^{\delta_{max}} \left(1 - \frac{\rho U}{(\rho U)_{max}}\right) dy, \quad (1)$$

$$\delta_2 = \int_0^{\delta_{max}} \frac{\rho U}{(\rho U)_{max}} \left(1 - \frac{U}{U_{max}}\right) dy, \quad (2)$$

where the upper integration limit δ_{max} is the local distance normal to the wall at which the velocity has a local maximum in the vicinity of the wall, referenced as U_{max}.

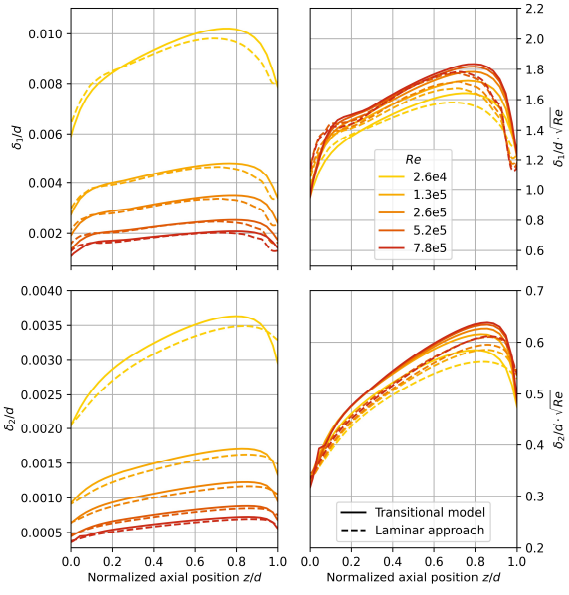

Figure 5: Normalized displacement and momentum thickness development in the cylindrical part of the nozzle (laminar region).

The normalized displacement and momentum thickness variation along the nozzle wall within the cylindrical part ($0 < z/d < 1$) for Reynolds numbers in the laminar region is shown in Figure 5. The computational results of the transitional model (solid line) are compared with a laminar approach (dashed line) by

Mickan et al. [8] based on integral methods for solving the boundary layer equations.

The curves of the transitional model and the laminar approach in the left-hand column (normalized by the throat diameter d) are in decent agreement. The values of the transitional model are slightly higher than predicted by the theoretical approach. All trendlines increase within the nozzle throat reaching a maximum value within the last quarter of the cylindrical part and then begin to decrease.

For higher Reynolds numbers, the values for δ_1/d and δ_2/d become smaller, where the highest reduction is visible between the two lowest Reynolds numbers. This is in line with the rise in discharge coefficient for increasing Reynolds numbers in the laminar range, according to the proportional relation between the C_D value and the effective reduction of the cross-sectional nozzle area by the displacement thickness:

$$C_D \sim \left(1 - \frac{2\,\delta_1}{d}\right)^2. \tag{3}$$

The curves show a self-similarity when multiplied by $\sqrt{Re}$ as can be seen in the right-hand column of Figure 5. This correlation corresponds to the Blasius solution for a laminar boundary layer of a flat plate.

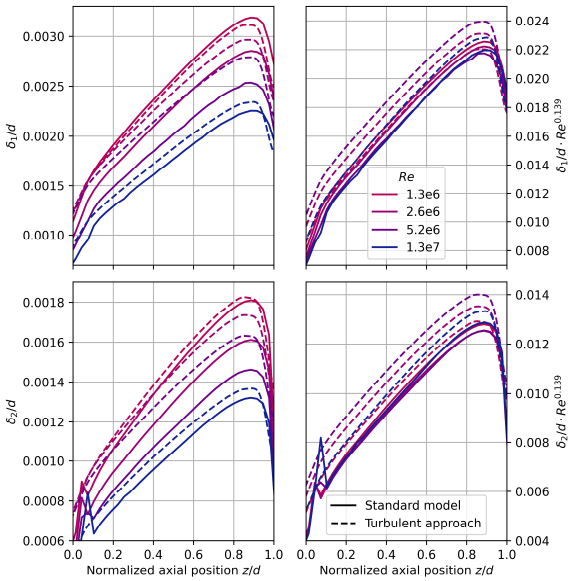

Figure 6: Normalized displacement and momentum thickness development in the cylindrical part of the nozzle (turbulent region).

Figure 6 shows the normalized displacement and momentum thickness curves for Reynolds numbers in the turbulent region (similarly to Figure 5 for the laminar region). The numerical results of the standard model (solid line) are compared with a turbulent approach (dashed line) by Mickan et al. [8] based on integral methods for solving the boundary layer equations.

The curves of the standard model and the turbulent approach in the left-hand column (normalized by the throat diameter d) are in good alignment. The values of the standard model are slightly below the theoretical prediction, except for the normalized displacement thickness at $Re = 1.3 \cdot 10^6$. As in the case for the laminar curves, the turbulent boundary layer thicknesses start to grow towards their maxima within the last quarter of the nozzle throat and then further decrease.

For rising Reynolds numbers, the boundary layer thickness diminishes. However, the reduction is smaller compared to the laminar curves for the same Reynolds number increase. This corresponds to the smaller slope for higher Reynolds numbers in the discharge coefficient diagram in Figure 3. The turbulent curves show a self-similarity when multiplied by $Re^{0.139}$ as can be seen in the right-hand column of Figure 6.

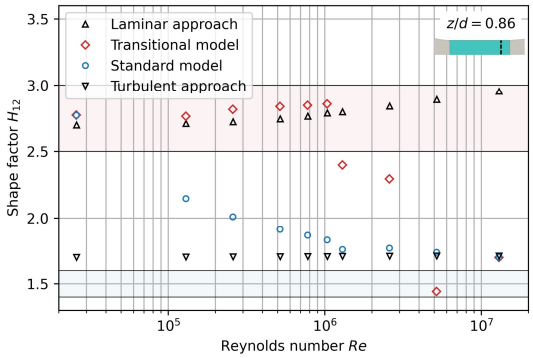

Figure 7: Shape factor H_{12} variation at the axial location z/d = 0.86 in the cylindrical part of the nozzle for different Reynolds numbers.

The shape factor H_{12} is defined as the ratio of displacement δ_1 to momentum thickness δ_2 of the boundary layer. Figure 7 illustrates the variation of the shape factor for different Reynolds numbers at the axial position $z/d = 0.86$ in the cylindrical part of the nozzle. The diagram shows the characteristic values of the theoretical approaches for laminar and turbulent flows [8], as well as the values of the standard and transitional model. Experimental investigations by Abu-Ghannam et al. [9] on the transition of the flow around a flat plate indicated characteristic regions for fully laminar and fully turbulent boundary layers in a range of 2.5 to 3.0 and 1.4 to 1.6, respectively. As a reference, these regions are highlighted in Figure 7 (light red and blue areas). The axial position $z/d = 0.86$ has been chosen for visualization, since this corresponds to the approximate location, where the displacement and momentum thickness are maximum (see Figure 5 and Figure 6).

The laminar approach predicts shape factors of ca. 2.7 to 3.0 with a slight increase towards higher Reynolds numbers. The turbulent approach, on the other hand, estimates values of 1.7 for all Reynolds numbers. These values are comparable with the measured data of a flat plate by Abu-Ghannam et al. [9]. Thus, the shape

factors of the laminar and turbulent approach indicate an upper and lower bound for the critical nozzle flow.

The shape factor, as calculated with the standard model, starts at values comparable with the laminar approach and then rapidly decreases, already for Reynolds numbers in the range of 10^5. It stagnates at a value of approximately 1.7, which corresponds to those of the turbulent approach.
The transitional model starts to follow the tendency of the shape factors as predicted by the laminar approach until approximately $Re = 10^6$. For Reynolds numbers above, a clear decline in shape factor is visible approaching values comparable to those of the standard model and turbulent approach.

In their experimental study of transitional boundary layers on a flat plate using hot-wire anemometry, Taghavi-Zenouz et al. [10] also showed this considerable decrease in the shape factor in a specific Reynolds number region. They identified this as the transitional region of the boundary layer. Thus, the transitional region for the investigated cylindrical nozzle can be estimated between $Re = 10^6$ and $5 \cdot 10^6$. This region is higher in comparison with the transitional regime estimated from the discharge coefficient of the experimental data ($8 \cdot 10^5 < Re < 2 \cdot 10^6$) in Figure 3. This implies a possibility to adjust the transitional model to experimental data of the shape factor as an important parameter to indicate the transitional region of the nozzle flow.

4. Conclusion

In this work, boundary layer effects in a cylindrical CFVN were investigated by means of numerical simulations. Two different approaches for modeling turbulence were used.
For the standard model, the discharge coefficients are in good agreement with experimental data only for high and low Reynolds numbers, but not in the intermediate regime. For the transitional model, on the other hand, the C_D values are in good accordance with the experiments for the entire Reynolds number range.
Typical laminar and turbulent boundary layer flows could be classified depending on the Reynolds number in terms of the displacement and momentum thickness development in the nozzle throat region. They are in decent accordance with theoretical approaches based on integral methods for solving the boundary layer equations.
Furthermore, the transitional Reynolds number region was estimated based on the drop of the shape factor in the nozzle throat from typical laminar to typical turbulent values according to respective literature. This predicted transitional region is higher than the experimental C_D curve suggests. This finding indicates a potential for improving the transitional model of the flow through critical nozzles based on the shape factor variation.

Acknowledgements

This work was supported through the Joint Research Project “Metrology infrastructure for high-pressure gas and liquified hydrogen flows”. This project (20IND11 MetHyInfra) has received funding from the EMPIR programme co-financed by the Participating States and from the European Union's Horizon 2020 research and innovation programme.

References

[1] ISO 9300: *Measurement of gas flow by means of critical flow Venturi nozzles*, 2005.
[2] B. Ünsal, K. R. Rathore, E. Koç, “Numerical Findings on the Boundary Layer Transition of Critical-Flow Venturi Nozzles”, in *Proceedings of FLOMEKO*, 2016.
[3] C. Wang, P. Cao, C. Li, H. Ding, L. Cui, “Influence of wall roughness on boundary layer transition position of the sonic nozzles”, *Measurement*, **139**, 196-204, 2019.
[4] M. A. Lambert, R. Maury, J.-C. Valière, E. Foucault, G. Lehnasch, “Experimental and numerical investigations on the shape and roughness of cylindrical critical flow venturi nozzles (CFVN)”, in *Proceedings of 19th International Congress of Metrology*, 2019.
[5] F. R. Menter, M. Kuntz, and R. Langtry, “Ten years of industrial experience with the SST turbulence model”, in *Proceedings of the fourth international symposium on turbulence, heat and mass transfer.* (Begell House), 625–632, 2003.
[6] R. B. Langtry, F. R. Menter, “Correlation-Based Transition Modeling for Unstructured Parallelized Computational Fluid Dynamics Codes”, *AIAA Journal*, **47**, 2894-2906, 2009.
[7] B. Mickan, J.-P. Vallet, C. Li, J. Wright, “Extended data analysis of bilateral comparisons with air and natural gas up to 5 MPa”, in *Proceedings of FLOMEKO*, 2016.
[8] B. Mickan, R. Kramer, D. Dopheide, “Determination of Discharge Coefficient of Critical Nozzles Based on Their Geometry and the Theory of Laminar and Turbulent Boundary Layers”, in *Proceedings of the 6th International Symposium on Fluid Flow Measurement*, 2006.
[9] B. J. Abu-Ghannam, R. Shaw, “Natural Transition of Boundary Layers – The Effects of Turbulence, Pressure Gradient, and Flow History”, *Journal of Mechanical Engineering Science*, **22**, 213-228, 1980.
[10] R. Taghavi-Zenouz, M. Salari, M. M. Tabar, E. Omidi, “Hot-wire anemometry of transitional boundary layers exposed to different freestream turbulence intensities”, in *Proceedings of the Institution of Mechanical Engineers Part G Journal of Aerospace Engineering*, 2008.